Research Article

Synthesis, growth, structural, optical and electrical properties of novel organic single crystal: *p*-toluidinium salicylate

Shanmugam Suresh[1], M. Nizam Mohideen[2], G. Vinitha[3], R. Mohan Kumar[1]

1 Department of Physics, Presidency College, Chennai, 600005, India

2 Department of Physics, The New College, Chennai, 600014, India

3 Department of Physics, SAS, VIT, Chennai, 600127, India

Corresponding author: *R. Mohan Kumar* (mohan66@hotmail.com)

Citation: Suresh S, Mohideen MN, Vinitha G, Kumar RM (2018) Synthesis, growth, structural, optical and electrical properties of novel organic single crystal: *p*-toluidinium salicylate. Modern Electronic Materials 4(3): 103–111. 10.3897/j.moem.4.3.33282

Abstract

A novel organic single crystal of *p*-toluidinium salicylate (PTSA) was grown by slow evaporation solution growth technique. The structure of grown crystal was determined from the single crystal X-ray diffraction analysis. The functional groups existing in PTSA crystal were accomplished by using Fourier transform infrared analysis. The optical transparency and band gap energy were estimated by utilizing the UV-Visible spectrum. Photoluminescence spectral studies revealed the photon excitation. The dielectric behavior of PTSA was investigated for different frequencies in a room temperature (308 K) environment. Third-order nonlinear optical susceptibility (χ^3) of PTSA crystal was elucidated by Z-scan measurements.

Keywords

crystal structure, dielectric, AC conductivity and resistivity, Z-scan analysis

1. Introduction

In the modern crystal science and technology, organic materials find wide application in telecommunication, optical limiting, optical data storage, ultrafast signal processes [1]. The donor-acceptor based intermolecular charge transfer organic molecular complex has high nonlinear optical properties due to the presence of delocalized π-electron system which enhance the asymmetric polarizability of the material. The molecular level organic compounds are expected to exhibit large values of molecular hyperpolarizability, if they possess polarizable electrons, for example, π-electrons spreading over a large distance.

It has been extended π-conjugated system with terminal donor-acceptor substituent to exhibit large values. Organic materials are known for their potential application in semiconductors, superconductors and nonlinear optical devices [2–3]. In addition, organic molecules also have a great attention owing to their potential application in the frontier areas such as nonlinear optics and light emitting diodes. Thus, the potential use of organic materials in optoelectronics has now become a serious matter. Organic single crystals with large π-electron delocalization are preferred for second and third order nonlinear optical applications. Because, optical nonlinearity depends on the crystal symmetry as the control of molecular orientation

in supramolecular structure is tedious and identified as a major obstacle in material's design. Many attempts have been made to control the structure of solids through charge transfer, hydrogen bond and π–π interactions. Generally, organic materials possess both donor and acceptor groups with a suitable conjugation path which leads to large third order nonlinearities. Due to the weakly base character of aniline complexes, *p*-toluidine (C_7H_9N) accepts the proton forming p-Toluidinium cation to enchance the NLO properties. The *p*-toluidine based crystals 4-methylanilinium *p*-toluenesulfonate, *p*-toludinium picrate have been reported [4–5]. Salicylic acid also known as 2-hydroxybenzoic acid is widely used as plant growth regulators and preservative in food products. It has antiseptic and anti-fungal properties and used widely in organic synthesis. The derivatives of salicylic acid compound have recently become attractive to experimentalists as well as theoreticians since their structure are some biological significance particularly in medical and enzyme chemistry [6]. The salicylic acid ($C_7H_6O_3$) donates the proton to the base and enhances the nonlinear property. The 3,5-dinitro salicylic acid monohydrate [7], Ammonium dihydrogen phosphate and Ammonium salicylate [8], Lithium salicylate [9], L-valinium salicylate [10] have been synthesized and their optical properties have been studied. In the crystal structure of the title compound: *p*-toluidinium saliylate ($C_7H_{10}N^+ \times C_7H_5O_3^-$) the cation and anion are linked via C–H–N- and C–H–O-interactions. In the present report, organic *p*-toluidinium salicylate **(PTSA)** was synthesized and crystal structure was solved for the first time. PTSA crystal was grown by slow evaporation solution growth technique and the structural and optical properties of the grown crystal were characterized by single crystal X-ray diffraction, Fourier transform infrared spectroscopic analysis, UV-Vis transmission spectral analysis, dielectric measurements and *Z*-scan studies.

2. Experimental

2.1 Material synthesis and crystal growth

PTSA was crystallized by slow evaporation process from *p*-toluidine (LOBA 99%) and salicylic acid (MERCK 99%) taking in equimolar ratio and the chemical reaction scheme of PTSA is illustrated in Fig. 1. The estimated amounts of the reactants were dissolved in double distilled water and solution was stirred for 6 h by using a magnetic stirrer to establish homogenous concentration in the solution. To improve the purity of the solution, Whatman filter papers were used to filter the solution and then it was transferred to a crystal growing utensil. The product was further purified by repeated recrystallization. The growth solution was prepared using the purified PTSA salt and it was kept in a constant temperature bath which was maintained at 36 °C. The colorless transparent single crystal of size about 11×5×3 mm³ obtained in 28 days is shown in Fig. 2.
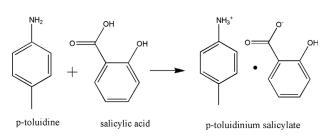

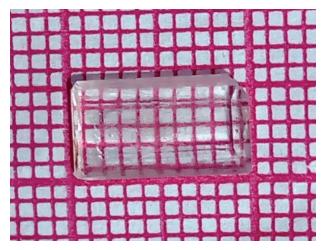**Figure 1.** Material synthesis scheme of *p*-toluidinium salicylate.

Figure 2. Photograph of as grown *p*-toluidinium salicylate crystal.

3. Results and discussion

3.1 Single crystal X-ray diffraction studies

The crystal structure of PTSA was determined by single crystal X-ray diffraction studies. The intensity data were collected using Bruker kappa APEXII single crystal X-ray diffractmeter with a graphite monochromated Mo*K*$_\alpha$ radiation (λ = 0.71073 Å) at 293 K [11]. The structure was solved by the direct method and refined by the full matrix least-squares technique on F2 employing the SHELXL 97 program package [12]. The crystallographic data of PTSA crystal is listed in Table 1. The asymmetric unit of the title compound comprises of a *p*-toluidine cation and a salicylate anion as shown in the ORTEP diagram (Fig. 3). The packing diagram of *p*-toluidine salicylate is shown in Fig. 4. The molecular formula of the crystal is $C_{14}H_{14}NO_3$. PTSA crystallizes in monoclinic crystal system with space group $P2_1/n$ which is a centro-symmetric. The calculated cell parameters are $a = 14.1940(16)$ Å, $b = 4.6883(6)$ Å, $c = 19.684(2)$ Å, $\alpha = \gamma = 90°$, $\beta = 90.613(3)°$ and volume $V = 1309.8(3)$ Å³.

The *p*-toluidine cation and salicylate anion are essentially planar, having a maximum deviation of 0.001(3) Å for atom C19 and 0.004(4) Å for atom C7, respectively. The dihedral angle between these two planes is about 36.3(2) Å, indicating that they are nearly parallel to each other. The C–N bond distance of NH2 group i.e., N1–C12 is 1.454 (3) Å, which is short for a C–N single bond, but still not quite as contracted as one would expect for a fully

Table 1. Crystal data and structure refinement for PTSA crystal.

Crystal data	Structure refinement
Identification code	PTSA
Empirical formula	$C_{14}H_{14}NO_3$
Formula weight	244.26
Temperature	293(2) K
Wavelength	0.71073 Å
Crystal system, space group	Monoclinic, $P2_1/n$
Unit cell dimensions	$a = 14.1940(16)$ Å, $\alpha = 90.00°$
	$b = 4.6883(6)$ Å, $\beta = 90.613(3)°$
	$c = 19.684(2)$ Å, $\gamma = 90.00°$
Volume	1309.8(3) Å^3
Z, Calculated density	4, 1.239 Mg/m^3
Absorption coefficient	0.088 mm^{-1}
F (000)	516
Crystal size	0.300 × 0.250 × 0.200 mm
Theta range for data collection	2.87 to 25.21 deg.
Limiting indices	$-16 \leq h \leq 16, -5 \leq k \leq 5, -23 \leq l \leq 23$
Reflections collected / unique	22018/2354 [R(int) = 0.0556]
Completeness to theta = 25.21	99.5 %
Absorption correction	Semi-empirical from equivalents
Refinement method	Full-matrix least-squares on F^2
Data / restraints / parameters	2354 / 0 / 166
Goodness-of-fit on F^2	0.951
Final R indices [$I > 2\text{sigma}(I)$]	$R_1 = 0.0572$, $wR_2 = 0.1687$
R indices (all data)	$R_1 = 0.1094$, $wR_2 = 0.2205$
Extinction coefficient	0.032(6)
Largest diff. peak and hole	0.377 and –0.302 e. Å^{-3}

Figure 4. The packing of the title compound, viewed extending along the b axis. Intermolecular hydrogen bonds are shows as dashed lines. H atoms not involved in hydrogen bonding have been omitted.
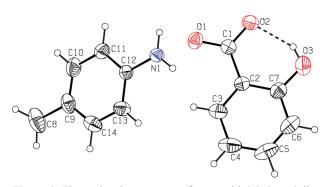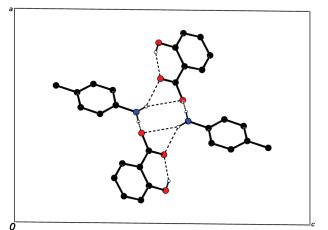

Figure 3. The molecular structure of atom with labels and displacement ellipsoids are drawn at the 50% probability level. In the anion (O3–H3A…O2), which generates an S(6) ring motif.

Table 2. Atomic coordinates (×10^4) and equivalent isotropic displacement parameters ($A^2 \times 10^3$) for PTSA crystal.

Atomic coordinates	x	y	z	U(eq)
C(1)	3396(2)	−1724(6)	4549(1)	50(1)
C(2)	2633(2)	22(6)	4245(1)	49(1)
C(3)	2789(2)	1533(7)	3651(2)	66(1)
C(4)	2107(3)	3307(8)	3379(2)	88(1)
C(5)	1256(3)	3536(9)	3706(3)	99(1)
C(6)	1081(3)	2052(10)	4281(2)	88(1)
C(7)	1757(2)	243(8)	4554(2)	63(1)
C(8)	6410(3)	1034(11)	1410(2)	106(2)
C(9)	6097(2)	1730(8)	2121(2)	68(1)
C(10)	6496(2)	409(9)	2673(2)	75(1)
C(11)	6217(2)	975(7)	3329(2)	63(1)
C(12)	5514(2)	2931(6)	3432(1)	47(1)
C(13)	5099(2)	4316(7)	2897(2)	63(1)
C(14)	5398(3)	3688(8)	2244(2)	72(1)
N(1)	5199(2)	3432(5)	4122(1)	51(1)
O(1)	4219(1)	−1574(4)	4304(1)	61(1)
O(2)	3220(1)	−3261(5)	5059(1)	70(1)
O(3)	1544(2)	−1240(7)	5117(1)	90(1)

established C═N. These bond length features are consistent with amino resonance form as it is commonly found for C–N single bonds involving sp^2 hybridized C and N atoms [13–14]. The bond distances of C1–O2, C1–O1 are 1.262(3) and 1.270(3) Å, respectively. It is clearly indicated the presence of C═O double bonds, including those generated through resonance.

In the crystal structure, intra as well as intermolecular hydrogen bonds could be observed. The intra-molecular hydrogen bonds are formed by the H atom of the alcoholic hydroxyl group as the donor and the carboxylic O atom of the carboxylic acid group as the acceptor in the salicylate anion (O3–H3A…O2), which generates an S(6) motif [15]. This motif is also observed in the crystal structure

of 2-aminopyridinium salicylate [16]. The intermolecular N–H…O hydrogen bond's interaction links the molecules into an infinite one-dimensional ribbon structure extending along the b-axis (Fig. 4.). The crystallographic data and structural refinement detail of PTSA crystal are given in Table 1. The atomic coordinates and equivalent isotropic displacement parameters for PTSA crystal are presented in Table 2. The bond length, bond angles and torsion angles are given in Tables 3, 4, respectively. The anisotropic displacement parameters for PTSA crystal are given in Table 5. The hydrogen coordinates and isotropic displacement parameters are presented in Table 6. The hydrogen bond interaction involved in the PTSA crystal is shown in Table 7.

Table 3. Bond lengths (Å) and angles (deg) for PTSA crystal.

Atomic coordinates	Bond lengths (Å) / angles (deg)	Atomic coordinates	Bond lengths (Å) / angles (deg)
C(1)–O(2)	1.262(3)	C(5)–C(6)–C(7)	120.4(4)
C(1)–O(1)	1.270(3)	C(5)–C(6)–H(6)	119.8
C(1)–C(2)	1.480(4)	C(7)–C(6)–H(6)	119.8
C(2)–C(3)	1.386(4)	O(3)–C(7)–C(6)	118.4(3)
C(2)–C(7)	1.394(4)	O(3)–C(7)–C(2)	122.0(3)
C(3)–C(4)	1.380(5)	C(6)–C(7)–C(2)	119.6(3)
C(4)–C(5)	1.379(6)	C(9)–C(8)–H(8A)	109.5
C(5)–C(6)	1.353(6)	C(9)–C(8)–H(8B)	109.5
C(6)–C(7)	1.385(5)	H(8A)–C(8)–H(8B)	109.5
C(7)–O(3)	1.346(4)	C(9)–C(8)–H(8C)	109.5
C(8)–C(9)	1.508(4)	H(8A)–C(8)–H(8C)	109.5
C(9)–C(10)	1.368(5)	H(8B)–C(8)–H(8C)	109.5
C(9)–C(14)	1.375(5)	C(10)–C(9)–C(14)	117.1(3)
C(10)–C(11)	1.380(4)	C(10)–C(9)–C(8)	121.1(4)
C(11)–C(12)	1.371(4)	C(14)–C(9)–C(8)	121.8(4)
C(12)–C(13)	1.366(4)	C(9)–C(10)–C(11)	122.4(3)
C(12)–N(1)	1.454(3)	C(9)–C(10)–H(10)	118.8
C(13)–C(14)	1.389(4)	C(11)–C(10)–H(10)	118.8
O(2)–C(1)–O(1)	121.6(3)	C(12)–C(11)–C(10)	118.9(3)
O(2)–C(1)–C(2)	119.2(3)	C(12)–C(11)–H(11)	120.6
O(1)–C(1)–C(2)	119.2(2)	C(10)–C(11)–H(11)	120.6
C(3)–C(2)–C(7)	118.8(3)	C(13)–C(12)–C(11)	120.9(3)
C(3)–C(2)–C(1)	120.1(3)	C(13)–C(12)–N(1)	120.6(3)
C(7)–C(2)–C(1)	121.1(3)	C(11)–C(12)–N(1)	118.5(2)
C(2)–C(3)–C(4)	121.2(3)	C(12)–C(13)–C(14)	118.6(3)
C(2)–C(3)–H(3)	119.4	C(12)–C(13)–H(13)	120.7
C(4)–C(3)–H(3)	119.4	C(14)–C(13)–H(13)	120.7
C(5)–C(4)–C(3)	118.6(4)	C(9)–C(14)–C(13)	122.2(3)
C(5)–C(4)–H(4)	120.7	C(9)–C(14)–H(14)	118.9
C(3)–C(4)–H(4)	120.7	C(13)–C(14)–H(14)	118.9
C(6)–C(5)–C(4)	121.4(4)	C(12)–N(1)–H(1A)	120.0
C(6)–C(5)–H(5)	119.3	C(12)–N(1)–H(1B)	120.0
C(4)–C(5)–H(5)	119.3	H(1A)–N(1)–H(1B)	120.0
		C(7)–O(3)–H(3A)	109.5

Table 5. Anisotropic displacement parameters ($A^2 \times 10^3$) for PTSA crystal.

Atomic coordinates	U_{11}	U_{22}	U_{33}	U_{23}	U_{13}	U_{12}
C(1)	57(2)	43(2)	50(2)	–4(1)	–2(1)	–3(1)
C(2)	52(2)	43(2)	51(2)	–5(1)	–6(1)	0(1)
C(3)	74(2)	59(2)	64(2)	7(2)	–14(2)	–8(2)
C(4)	103(3)	70(3)	91(3)	24(2)	–37(2)	–10(2)
C(5)	79(3)	79(3)	138(4)	5(3)	–41(3)	15(2)
C(6)	61(2)	92(3)	112(3)	–8(3)	–12(2)	16(2)
C(7)	60(2)	66(2)	64(2)	–10(2)	–5(2)	1(2)
C(8)	120(3)	132(4)	67(2)	–25(2)	28(2)	–41(3)
C(9)	71(2)	74(2)	58(2)	–13(2)	14(2)	–26(2)
C(10)	65(2)	85(3)	74(2)	–14(2)	17(2)	9(2)
C(11)	58(2)	67(2)	63(2)	0(2)	2(1)	13(2)
C(12)	46(2)	45(2)	49(2)	–1(1)	1(1)	–4(1)
C(13)	72(2)	58(2)	59(2)	6(2)	–5(2)	7(2)
C(14)	89(2)	73(2)	54(2)	7(2)	–7(2)	–10(2)
N(1)	55(1)	52(2)	47(1)	2(1)	2(1)	13(1)
O(1)	55(1)	50(1)	78(2)	2(1)	9(1)	5(1)
O(2)	64(1)	82(2)	64(1)	20(1)	–8(1)	–7(1)
O(3)	71(2)	124(3)	76(2)	4(2)	16(1)	2(2)

Table 4. Torsion angles (deg) for PTSA crystal.

Atomic coordinates	Torsion angles (deg)
O(2)–C(1)–C(2)–C(3)	–174.5(3)
O(1)–C(1)–C(2)–C(3)	7.6(4)
O(2)–C(1)–C(2)–C(7)	7.2(4)
O(1)–C(1)–C(2)–C(7)	–170.7(3)
C(7)–C(2)–C(3)–C(4)	2.2(5)
C(1)–C(2)–C(3)–C(4)	–176.2(3)
C(2)–C(3)–C(4)–C(5)	–0.5(5)
C(3)–C(4)–C(5)–C(6)	–0.4(6)
C(4)–C(5)–C(6)–C(7)	–0.3(7)
C(5)–C(6)–C(7)–O(3)	–178.5(4)
C(5)–C(6)–C(7)–C(2)	1.9(6)
C(3)–C(2)–C(7)–O(3)	177.6(3)
C(1)–C(2)–C(7)–O(3)	–4.1(5)
C(3)–C(2)–C(7)–C(6)	–2.8(5)
C(1)–C(2)–C(7)–C(6)	175.5(3)
C(14)–C(9)–C(10)–C(11)	0.2(5)
C(8)–C(9)–C(10)–C(11)	–179.2(3)
C(9)–C(10)–C(11)–C(12)	0.1(5)
C(10)–C(11)–C(12)–C(13)	–0.4(5)
C(10)–C(11)–C(12)–N(1)	177.6(3)
C(11)–C(12)–C(13)–C(14)	0.4(5)
N(1)–C(12)–C(13)–C(14)	–177.5(3)
C(10)–C(9)–C(14)–C(13)	–0.2(5)
C(8)–C(9)–C(14)–C(13)	179.2(3)
C(12)–C(13)–C(14)–C(9)	–0.1(5)

Table 6. Hydrogen coordinates ($\times 10^4$) and isotropic displacement parameters ($A^2 \times 10^3$) for PTSA crystal.

Hydrogen coordinates	x	y	z	U(eq)
H(3)	3364	1349	3433	79
H(4)	2219	4327	2982	106
H(5)	794	4735	3529	119
H(6)	503	2249	4493	106
H(8A)	6104	2298	1094	159
H(8B)	6244	-901	1304	159
H(8C)	7080	1262	1381	159
H(10)	6972	-919	2604	90
H(11)	6501	46	3695	75
H(13)	4625	5650	2968	76
H(14)	5117	4622	1878	86
H(1A)	4747	4608	4196	62
H(1B)	5465	2551	4456	62
H(3A)	1989	-2270	5222	135

3.2 FTIR spectral studies

The FTIR spectrum of PTSA crystal was recorded in the range 4000 – 400 cm^{-1} by using KBr pellet technique and the presence of various functional groups in the grown PTSA has been elucidated as shown in Fig. 5. The characteristic vibrational frequencies were assigned and presented in Table 8. The functional groups of PTSA such as asymmetric and symmetric stretchings of N–H in the amino (NH$_3$$^+$) observed at the wave numbers 3496 and

Table 7. Hydrogen bonds for PTSA (Å and deg) crystal.

D–H...A	d(D–H)	d(H...A)	d(D...A)	<(DHA)
O(3)–H(3A)...O(2)	0.82	1.84	2.564(3)	146.6
N(1)–H(1A)...O(1)[#1]	0.86	1.95	2.749(3)	153.4
N(1)–H(1B)...O(1)[#2]	0.86	2.52	3.315(3)	154.2
N(1)–H(1B)...O(2)[#2]	0.86	2.12	2.751(3)	130.4

Symmetry transformations used to generate equivalent atoms: #1 $x, y + 1, z$ #2 $-x + 1, -y, -z + 1$

Table 8. FT-IR spectral assignment of PTSA crystal.

Wavenumber (cm^{-1})	Assignments
3496	Amino N–H asymmetric stretching (NH$_3^+$)
3354	Amino N–H symmetric stretching (NH$_3^+$)
2849	C–H stretching medium
2927	Methyl C–H symmetric stretching (CH$_3$)
2552	Carboxylic acid C=O and O–H stretch
1429	Methyl C–H asymmetric bending
1751	Aromatic ring C=C stretch
1919	C=N stretching vibration
910	Stretching of C–C
613	Wagging of COO$^-$

3354 cm^{-1}, respectively. The presence of methyl groups was confirmed through the symmetric and asymmetric stretching vibrations of C–H at 2927 and 1429 cm^{-1} respectively. The sharp peaks observed at 2849 cm^{-1} is due to the stretching of C–H. The peak observed at 1751 cm^{-1} is due to the stretching of C=C in the aromatic ring and the peak noted at 1919 cm^{-1} is due to C=N stretching vibration. The C–C stretching and COO$^-$ wagging peaks observed at 910 and 613 cm^{-1} respectively [17–18]. The carboxyl group (COOH) of PTSA was confirmed at the wave number 2552 cm^{-1}. Hence, the presence of functional groups confirmed the formation title compound.

3.3 Optical transmittance studies

UV-Vis spectral analysis provides an essential structural knowledge due to UV and visible light absorption and it is also associated with the shifting of the electrons from the ground to the higher energy states of π- and σ-orbitals [2]. UV-Vis transmission spectrum recorded in the range 200–800 nm is shown in Fig. 6. It is seen from the spectrum that PTSA crystal has a very low cut-off wavelength around 320 nm with transparency around 65%. The absorption coefficient (α) can be determined from the transmission spectrum based on the relation,

$$\alpha = \frac{\text{ùùù}}{t} \log\left(\frac{}{T}\right), \qquad (1)$$

where T is the transmittance and 't' is the thickness of the crystal. The optical band gap was estimated from the transmission spectrum and the optical absorption coefficient (α) near the absorption edge was calculated using the relation,

$$(\alpha h\nu)^2 = A(E_g - h\nu), \qquad (2)$$

where E_g is the optical band gap of the crystal and A is a constant. The variation of $(\alpha h\nu)^2$ with '$h\nu$' in the fundamental absorption region was plotted as shown in Fig. 7. The band gap of PTSA crystal estimated by extrapolation of the linear part of the graph is 3.2 eV. The band gap and transmittance in the entire visible region enables the crystal suitable for optoelectronic and photonics applications [19].

3.4 Photoluminescence studies

Photoluminescence **(PL)** spectral investigation is one of the most competent mechanisms which impart compara-
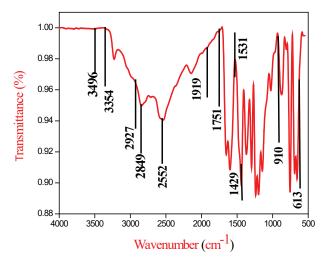

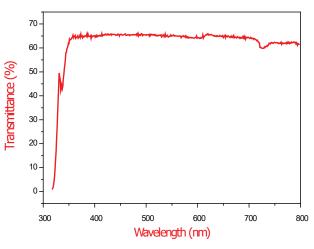**Figure 5.** FTIR spectrum of PTSA crystal.

Figure 6. UV-Vis transmission spectrum of PTSA crystal.

tively direct knowledge regarding the materials' physical properties at the molecular level, which also includes the defects in deep and shallow level mechanisms and energy gap states. The emission occurs because of the radioactive recombination of electron and hole pair, that is specially necessary for the mechanism of laser in the visible range and it is meant for chromophores in the case of organic crystals [2]. Figure 8 shows the
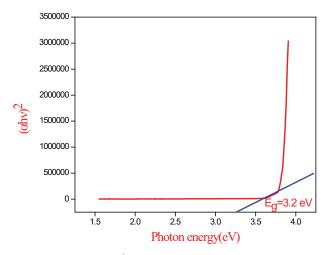
Figure 7. Plot of $(\alpha h\nu)^2$ vs. photon energy of PTSA crystal.

Figure 8. Emission spectrum of PTSA crystal.

room temperature PL spectrum of PTSA crystal and the broad photoluminescence emission **(PLE)** peak seen in the spectrum at 440 nm is due to interaction between the electronic system of the luminescent center and the vibrations of ions. Such a broad PL emission caused by diverse electronic transitions occurring in different energy levels is due to deep or shallow holes with in the band gap [20]. The deep holes are origin states for the green, yellow, orange and red PL emissions, while the shallow holes are responsible for the violet and blue emissions [21]. The broad PL emission observed at 440 nm violet emission is an indicative of the charge transfer process as well as the trapping of electrons and it is due to the contribution of the shallow holes than the deep holes [22]. Thus, PLE spectrum reveals that PTSA crystal exhibits blue shift emission, which is most useful for luminescent applications.

3.5 Dielectric studies

Dielectric properties are correlated with the electro-optic property of the crystals [23]. The dielectric constant and dielectric loss of the grown single crystal was measured as a function of frequency from 50 Hz to 3 MHZ. The polished PTSA crystal faces were coated with silver paste and mounted between the two copper electrodes to form a parallel plate capacitor. The dielectric constant (ε_r) of the sample was calculated using the relations,

$$\varepsilon_r = \frac{Ct}{\varepsilon_0 A},\qquad(3)$$

$$\tan \delta = \varepsilon_r D \qquad(4)$$

where C is the capacitance, t is the thickness of the crystal, ε_0 is the permittivity of free space, D is the dissipation factor and A is the area of the crystal. The variation of dielectric constant as a function of frequency at room temperature is shown in Fig. 9. The high value of dielectric constant at low frequencies are due to the presence of
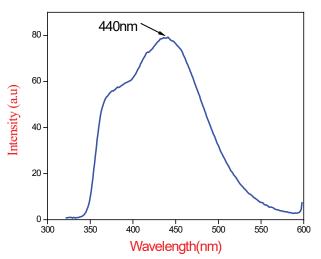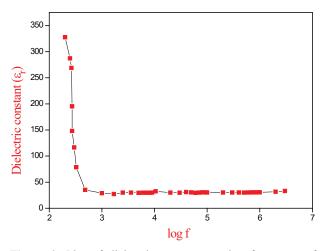

Figure 9. Plot of dielectric constant vs. log frequency of PTSA crystal.

electronic, ionic, dipolar and space charge polarizations, and its low value at high frequencies be due to loss of these polarizations gradually [24]. The dielectric loss observed as a function of frequency at room temperature is shown in Fig. 10. The dielectric loss value decreased at high frequencies. The low values of dielectric constant with minimized dielectric loss at higher frequencies of the grown single crystal shows enhanced optical quality with lesser defects and it suggests that the PTSA single crystals are useful for devices applications.

3.6 Study of AC conductivity and resistivity

The effect of frequency and temperature on AC conductivity offers a lot of information about the bound electric charge carriers. This leads to good explanation and understanding of the electric behavior of organic semiconductors [25]. The AC conductivity was calculated using the relation,

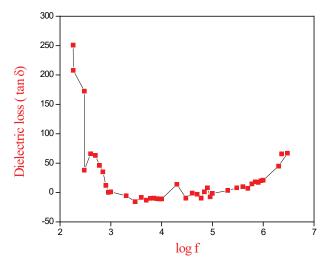$$\sigma_{ac} = 2\pi f\varepsilon_0\varepsilon_r\tan \delta,\qquad(5)$$

Figure 10. Plot of Dielectric loss vs. log frequency of PTSA crystal.

Figure 11. Plot of AC Conductivity vs. log frequency of PTSA crystal.

where, f is the frequency of applied field. The plot of AC conductivity versus frequency at room temperature is shown in Fig. 11. It shows that at a given temperature, the magnitude of conductivity is high at high frequencies which is a normal dielectric behavior. The electrical conduction in dielectrics is mainly a defect controlled process in the room temperature environment. It is clear that the AC conductivity increases and resistivity decreases with increase of frequency. Fig. 12 shows the resistivity of material for different frequency measured at room temperature. It shows that there is a relationship between the relative charge in temperature with the two electrical factors; conductivity and resistivity. The resistivity was calculated using the relation,

$$\rho = 1/2\pi f \varepsilon_0 \varepsilon_r \tan \delta, \qquad (6)$$

where, ρ is the resistivity and ω is angular frequency of applied electric field. However, the electrical conductivity varied in the opposite direction of resistivity. The PTSA single crystal showed good optical quality with lesser defects and it suggests that the PTSA crystal will be useful for device applications.

3.7 Z-scan measurement

The third order nonlinear optical characteristics of PTSA were accomplished by means of the process of Z-scan. This approach facilitates the concurrent measurement of magnitude as well as sign of the nonlinear refractive index (n_2) and the nonlinear absorption (β) using the open and closed configurations of Z-scan. In the present investigation, Nd–YAG laser was used to assess the third order nonlinearity of PTSA.

From the obtained data of Z-scan, the difference between the normalized valley and peak transmittance ΔT_{p-v} can be evaluated by using the relation,
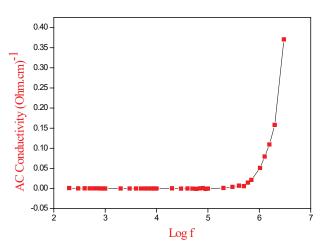
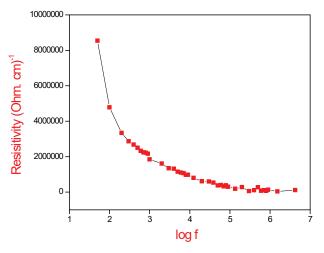$$\Delta T_{p-v} = 0.406(1-S)^{0.25}|\varphi|, \qquad (7)$$

Figure 12. Plot of resistivity vs. log frequency of PTSA crystal.

where, $|\varphi|$ signifies the on-axis phase shift at the focus and S denotes the aperture linear transmittance, which can be estimated using the relation,

$$S = 1 - \exp\left(-\frac{2r_a^2}{\omega_a^2}\right), \qquad (8)$$

where r_a indicates the aperture radius and ω_a represents the radius at the aperture.

The on-axis phase shift $|\varphi|$ is given by,

$$|\varphi| = kn_2 L_{eff} I_0, \qquad (9)$$

where $L_{eff} = (1 - e^{-\alpha L})/\alpha$, L stands for the length of the used sample, I_0 denotes the laser intensity at focus $z = 0$, α indicates the linear absorption coefficient and k is the wave number ($k = 2\pi/\lambda$).

The nonlinear absorption is reckoned by utilizing the data obtained from the open aperture Z-scan and is given by,

$$\beta = \frac{2\sqrt{2}\Delta T}{I_0 L_{eff}}, \qquad (10)$$

ΔT is the maximum value of the open aperture normalized transmittance obtained from the Z-scan plot. The nonlinear absorption coefficient (β) exhibits a negative value for saturation absorption and positive in the case of two photon absorption. The real and imaginary part of nonlinear optical susceptibility (χ^3) were evaluated from the experiment data of 'n_2' and 'β' values.

$$\mathrm{Re}\,\chi^{(3)}(\mathrm{esu}) = \frac{10^{-4}\left(\varepsilon_0 C^2 n_0^2 n_2\right)}{\pi}\,(\mathrm{cm}^2/\mathrm{W}) \qquad (11)$$

$$\mathrm{Im}\,\chi^{(3)}(\mathrm{esu}) = \frac{10^{-2}\left(\varepsilon_0 C^2 n_0^2 \lambda \beta\right)}{4\pi^2}\,(\mathrm{cm}/\mathrm{W}) \qquad (12)$$

where, ε_0 denotes the vacuum permittivity and C represents the velocity of light in vacuum. The absolute third order nonlinear optical susceptibility $|\chi^{(3)}|$ is given by

$$\left|\chi^{(3)}\right| = \sqrt{\left(\mathrm{Re}\,\chi^{(3)}\right)^2 + \left(\mathrm{Im}\,\chi^{(3)}\right)^2}. \qquad (13)$$

it is observed that the closed aperture Z-scan curve of PTSA discloses the peak to valley configuration as well as it is an evidence for negative nonlinearity as illustrated in Fig. 13. This is also represented as self-defocusing effect which takes place due to the dependence of refractive index with temperature [26] and finds application in the domain of fabricating optical sensors [27]. The open aperture configuration of Z-scan is displayed in Fig. 14. The nonlinear absorption coefficient (β) is found to be 0.02×10^{-4} cm/W and it signifies the process of saturable absorption and it is widely used for the application of optical power limiting process [26]. The obtained Z-scan data measurement precisely illustrates that PTSA shows the third order nonlinear optical characteristics and enumerated in Table 9. The third order susceptibility of PTSA was compared with other reported acentric crystals and listed in Table 10. The nonlinear refraction and absorption are attributed to self-defocusing nature and two photon absorption process of PTSA respectively.

4. Conclusion

A novel organic material p-toluidinium salicylate was synthesized and single crystal of PTSA was grown by slow evaporation method. The molecular structure was analyzed by using single crystal X-ray diffraction studies. The single crystal data indicates that the PTSA crystallizes in monoclinic crystal system with centro-symmetric space group $P2_1/n$. The existence of diverse functional groups was identified from the FTIR spectral studies. The transmittance in the visible region had the lower cutoff wavelength of 320 nm and the band gap energy of PTSA was estimated to be 3.2 eV. The photoluminescence spectral study disclosed the electron excitation of PTSA. The dielectric constant and dielectric loss of PTSA crystal were studied with different frequency at room temperature. The nonlinear optical parameters were evaluated by closed and open Z-scan
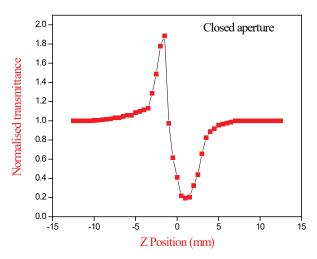

Figure 13. Z-scan curve traced in closed aperture mode for PTSA crystal.
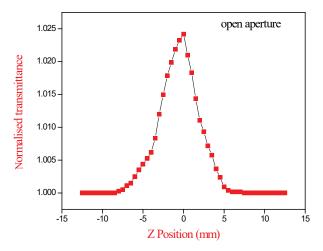

Figure 14. Z-scan curve traced in open aperture mode for PTSA crystal.

Table 9. Third order nonlinear optical parameters of PTSA crystal.

Nonlinear parameters	Measured values
Nonlinear refractive index (n_2)	9.39×10^{-8} cm^2/W
Nonlinear absorption coefficient (β)	0.02×10^{-4} cm/W
Real susceptibility ($\chi_R^{(3)}$)	10.13×10^{-6} esu
Imaginary susceptibility ($\chi_I^{(3)}$)	0.12×10^{-6} esu
Absolute susceptibility ($\chi^{(3)}$)	10.13×10^{-6} esu

Table 10. Comparison of $\chi^{(3)}$ values of PTSA with other NLO materials.

Crystal	Third order susceptibility $\chi^{(3)}$ (esu)	Reference
PTSA	10.13×10^{-6}	Present Work
LAPA	5.24×10^{-7}	[28]
VMST	9.69×10^{-12}	[29]
GUCN	2.05×10^{-8}	[30]

signature technique. Thus, the various characterization of PTSA crystal proved its suitability for the future photonic and optoelectronic device fabrication.

References

1. Zong Y., Shao H., Pang Y., Wang D., Liu K., Wang L. Multicomponent hydrogen-bonding organic solids constructed from 6-hydroxy-2-naphthoic acid and N-heterocycles: Synthesis, structural characterization and synthon discussion. *J. Mol. Struct.* 2016; 115: 187–198. https://doi.org/10.1016/j.molstruc.2016.02.095

2. Nageshwari M., Rathika Thaya Kumari C., Vinitha G., Peer Mohamed M., Sudha S., Lydia Caroline M. Crystal growth, structureal, spectral, thermal, dielectric, linear and nonlinear optical characteristics of a new organic acentric material: L-Methionine-Succinic acid (2/1). *J. Mol. Struct.* 2018; 1155: 101–109. https://doi.org/10.1016/j.molstruc.2017.10.099

3. Sankar S., Manikandan M.R., Ram S.G., Mahalingam T., Ravi G. Gel growth of α and γ-glycine and their characterization. *J. Cryst. Growth.* 2010; 312: 2729–2733. https://doi.org/10.1016/j.jcrysgro.2010.04.051

4. Shanmugam G., Brahadeeswaran S. Spectroscopic, thermal and mechanical studies on 4-methlanilinium *p*-toluenesulfonate a new organic NLO single crystal. *Spectrochim. Acta A Mol. Biomol. Spectrosc.* 2012; 95: 177–183. https://doi.org/10.1016/j.saa.2012.04.100

5. Muthu K., Meenakshisundaram S. Crystal growth, structure and characterization of *p*-toluidinium picrate. *J. Cryst. Growth.* 2012; 352: 163–166. https://doi.org/10.1016/j.jcrysgro.2011.11.058

6. Kwon Y. Theoretical study on salicylic acid and its analogues: intromolecular hydrogen bonding. *J. Mol. Struct.* 2000; 532: 227–237. https://doi.org/10.1016/S0166-1280(00)00555-8

7. Mathammal R., Sangeetha K., Guru Prasad L., Jayamani V. Crystal growth, structural characterization and theoretical investigation on 3,5-dinitro salicylic acid monohydrate for nonlinear optical applications. *Spectrochim. Acta A Mol. Biomol. Spectrosc.* 2015; 144: 200–214. https://doi.org/10.1016/j.saa.2015.01.117

8. Voronov A.P., Salo V.I., Puzikov V.M., Babenko G.N., Roshal A.D., Tkachenko V.F. Hybrid organic-inorganic crystals based on ammonium dihydrogen phosphate andammonium salicylate. *J. Cryst. Growth.* 2011; 335: 84–89. https://doi.org/10.1016/j.jcrysgro.2011.08.018

9. Zaitseva N., Newby J., Hull G., Saw C., Carman L., Cherepy N., Payne, Synthesis S. Growth and properties of lithium salicylate single crystals. *Cryst. Growth Des.* 2009; 9: 3799–3802. https://doi.org/10.1021/cg9005289

10. Andal C., Murugakoothan P. Growth and characterization of organic nonlinear optical crystal: L-valinium salicylate. *J. Opt.* 2014; 125: 2713–2715. https://doi.org/10.1016/j.ijleo.2013.11.026

11. Bruker, APEX2, SAINT, XPREP, and SADABS. Bruker AXS Inc, Madison (Wiscosin, USA), 2004.

12. Sheldrick G.M. A short history of SHELX. *Acta Cryst.* 2008; A64: 112–122. https://doi.org/10.1107/S0021889811043202

13. Oueslati A., Kefi R., Ben Nasr C., Lefebvre F. Crystal structure of a new organic hydrogenmonophosphate adduct [2-NH$_2$-6-CH$_3$-CH$_4$CH$_3$N$_2$O]$_2$ HPO$_4$. *J. Mol. Struct.* 2007; 871(1–3): 49–58. https://doi.org/10.1016/j.molstruc.2007.01.050

14. Sethuram M., Bhargavi G., Dhandapani M., Amithaganesan G., Nizam Mohideen M. N2(4-methoxysalicylidene; arginine hermihydrate. *Acta Cryst.* 2013; E69: 1301–1302. https://doi.org/10.1107/S1600536813019727

15. Bernstein J., Devis R.E., Shimoni L., Chang N.L. Patterns in hydrogen bonding: functionality and graph set analysis in crystals. *Angew. Chem. Int. Ed. Engl.* 1995; 34: 1555–1573. https://doi.org/10.1002/anie.199515551

16. Jin Z.M., Pan Y.J., Hu M.L., Shen L. Crystal structure of 2-amino-3-methylpyridinium ortho-phthalate, *J. Chem. Crystallogr.* 2001; 31: 191–195. https://doi.org/10.1023/A:1014391031842

17. Silverstine R.M., Webster F.X. Spectrometric identification of organic compounds, Singapore: John Wiley and Sons Publishers, 2004.

18. Ramachandra Raja C., Antony Joseph A. Crystal growth and characterization of new nonlinear optical single crystals of l-alaninium fumarate, *J. Mater. Lett.* 2009; 63: 2507–2509. https://doi.org/10.1016/j.matlet.2009.08.046

19. Prasad L.G., Krishnakumar V., Nagalakshmi R., Manohar S. Physicochemical properties of highly efficient organic NLO crystal: 4-Aminobenzamide. *Mater. Chem. Phys.* 2011; 128: 90–95. https://doi.org/10.1016/j.matchemphys.2011.02.043

20. Liu Y., Li M., Fang Q., Lv Q., Wu M., Cao S. Structural and photoluminescence properties of polyethylene glycol (PEG)-assisted growth co-doped ZnO nanorod arrays compared with pure ZnO nanorod arrays. *Chinese J. Phys.* 2010; 48: 523–531. https://doi.org/10.6122/CJP

21. Cavalcante L.S., Sczancoski J.C., De Vicente F.S., Frabbro M.T., Siu Li M., Varela J.A., Longo E. Microstructure, dielectric properties and optical band gap control on the photoluminescence behavior of Ba [Zr$_{0.25}$Ti$_{0.75}$]O$_3$ thin films. *J. Sol-Gel. Sci. Technol.* 2009; 49(1): 35–46. https://doi.org/10.1007/s10971-008-1841-x

22. Sczancoski J.C., Cavalcante L.S., Badapanda T., Rout S.K., Panigrahi S., Mastelaro V.R., Varela J.A., Siu Li M., Longo E. Structure and optical properties of [Ba$_{1-x}$Y$_{2x/3}$] (Zr$_{0.25}$Ti$_{0.75}$)O$_3$ powders. *Solid State Sci.* 2010; 12: 1160–1167. https://doi.org/10.1016/j.solidstatesciences.2010.04.002

23. Boomadevi S., Dhanasekaran R. Synthesis, crystal growth and characterization of L-pyrrolidone-2-carboxylic acid (L-PCA) crystals. *J. Cryst. Growth.* 2004; 261(1): 70–76.

24. Gill A.S., Kalainathan S. Thermal, optical, mechanical and dielectric properties of nonlinear optical crystal 4-methoxy benzaldehyde-N-methyl 4-stilbazolium tosylate. *J. Phys. Chem. Solids.* 2011; 72: 1002–1007. https://doi.org/10.1016/j.jpcs.2011.04.017

25. Senturk E. Dielectric characteristics of a Ce^{3+}-doped Sr$_{0.61}$Ba$_{0.39}$Nb$_2$O$_6$ single crystal with Cole-Cole plots technique. *J. Solid State Chem.* 2004; 177: 1508–1512. https://doi.org/10.1016/j.jssc.2003.12.001

26. Jayaprakash P., Sangeetha P., Rathika Thaya Kumari C., Lydia Caroline M. Investigation on the growth, spectral, lifetime, mechanical analysis and third-order nonlinear optical studies of L-Methionine admixtured D-Mandelic acid single crystal: a promising material for nonlinear optical applications. *Physica B: Condens. Matter.* 2017; 518: 1–38. https://doi.org/10.1016/j.physb.2017.05.017

27. Nageshwari M., Jayaprakash P., Rathika Thaya Kumari C., Vinitha G., Lydia Caroline M. Growth, spectral, linear and nonlinear optical characteristics of an efficient semiorganic ancentric crystal: L-Valinium L-Valine Chloride. *Physica B: Condens. Matter.* 2017; 511: 1–9. https://doi.org/10.1016/j.physb.2017.01.027

28. Jothi Mani R., Selvarajan P., Alex Devadoss H., Shanthi D. Second-order, third-order NLO and other properties of L-alanine crystals admixtured with perchloric acid (LAPA). *J. Opt.* 2015; 126(2): 213–218. https://doi.org/10.1016/j.ijleo.2014.08.143

29. Krishna Kumar M., Sudhahar S., Pandi P., Bhagavanaarayana G., Mohan Kumar R. Studies of the structural and third-order nonlinear optical properties of solution grown 4-hydroxy-3-methoxy-4'-N'-methylstilbazolium tosylate monohydrate crystals. *Opt. Mater.* 2014; 36: 988–995. https://doi.org/10.1016/j.optmat.2014.01.007

30. Dhavamurthy M., Raja R., Syed Suresh Babu K., Mohan R. Crystal structure, growth and characterization of a novel organic third-order nonlinear optical crystal: Guanidinium cinnamate. *Appl. Phys. A.* 2016; 122: 734. https://doi.org/10.1007/s00339-016-0219-0